Received: 23 May 2024 | Revised: 17 October 2024 | Accepted: 18 October 2024

DOI: 10.1002/pamm.202400129

RESEARCH ARTICLE

The mixed displacement method to avoid shear locking in problems in elasticity

Tarun Kumar Mitruka Vinod Kumar Mitruka | **Manfred Bischoff**

University of Stuttgart, Institute for Structural Mechanics, Stuttgart, Germany

Correspondence
Tarun Kumar Mitruka Vinod Kumar Mitruka, University of Stuttgart, Institute for Structural Mechanics, Pfaffenwaldring 7, 70550 Stuttgart, Germany.
Email: mitruka@ibb.uni-stuttgart.de

Funding information
Deutsche Forschungsgemeinschaft, Grant/Award Number: BI 722/12-1

Abstract

The mixed displacement (MD) method was initially developed to mitigate geometrical locking effects in beams, plates, and shells with the intention of having intrinsically locking-free characteristics while using equal-order interpolation for all degrees of freedom. In other words, it is an unlocking scheme that works independent of the element shape, polynomial order, and discretization scheme. It includes additional degrees of freedom that adhere to a carefully designed differential relation that can be interpreted as a kinematic law, incorporated in a mixed sense. Certain constraints are to be enforced on these additional degrees of freedom to obtain a well-posed system of equations. In this work, the MD method is extended for problems in solid mechanics. We present the underlying variational formulation, followed by its application to 2D solid elements. Additionally, we showcase an idea to enforce the additional constraints in a general sense. Various numerical examples, within the framework of the finite element method and isogeometric analysis, are outlined to demonstrate the performance of the MD method in the geometrically linear and geometrically nonlinear cases.

1 | INTRODUCTION

Over the last six decades, various strategies have been adopted in the context of the finite element method (FEM) to address the issue of locking. For instance, it was observed that using a lower number of integration points leads to locking-free finite elements, resulting in the method of reduced integration [1–3]. This method was then generalized to a so-called B-bar method, where the strain-displacement matrix is decomposed into a dilatational and a deviatoric part, which are then modified to obtain a locking-free formulation [4]. In connection with the treatment of transverse shear locking in plates and shells [5] and [6], developed the assumed natural strain (ANS) method, which includes computation and interpolation of tying points within the element to obtain a modified strain function. Afterwards, a new class of finite elements was developed that included additional enhanced strain fields to treat geometric and material locking effects. This is the enhanced assumed strain (EAS) method [7, 8]. Later, the discrete strain gap (DSG) method [9, 10] was invented, which is a unified approach that helps to alleviate all types of geometrical locking effects. It has to be noted that the number of methods to treat locking and its corresponding literature is rich, and not everything is mentioned here. These approaches are effective in producing locking-free finite elements; however, as the discretization methods diversify, their

extensions are rather not straightforward. In other words, the process of developing these unlocking schemes has to be revisited when utilizing, for instance, Isogeometric Analysis (IGA), collocation methods, or meshless methods. In this work, emphasis is given only to FEM and IGA.

The idea of IGA [11] is to make use of the underlying spline functions from CAD (Computer-Aided Design) geometry as shape functions within the finite element method. Even though spline functions have higher continuity and are smoother than standard Lagrangian function spaces, the problem of locking reappears while using them as an ansatz. This led to the process of again developing feasible unlocking schemes. For example, in the context of IGA, Adam et al. [12, 13] devised rules to perform reduced integration; Elguedj et al. [14] revisited the B-bar method; Caseiro et al. [15] explored the extension of the ANS method; Cardoso and Cesar De Sa [16] rediscovered the EAS method; and Echter and Bischoff [17] reconstructed the DSG method. Thus, motivated by the goal of developing an unlocking scheme that works independently of the polynomial order, element shape, and discretization method, two sets of intrinsically locking-free formulations evolved. They are the *Hierarchic Formulations* (HF) and the *Mixed Displacement* (MD) method. These intrinsically locking-free formulations are built on the principle of using equal-order interpolation of all the fields involved, thereby avoiding the creation of special "lower order spaces" in order to avoid locking effects. This is triggered by the spirit of IGA, where the desire is to avoid the meshing procedure by using the function spaces of the geometry directly for approximating the unknown fields. The hierarchic formulations are based on the reparameterization of the governing kinematic equations and were developed to alleviate transverse shear locking effects in beams, plates, and shells. In particular, Echter et al. [18] showed that using transverse shear strains as an independent field instead of rotations can lead to a locking-free formulation, but they exhibit oscillations in stress resultants near the boundary. This is called a hierarchic rotation formulation. Later, Oesterle et al. [19, 20] demonstrated that decomposing the transverse displacement into its bending and shear parts and using them as independent fields instead of transverse shear strains results in a locking-free and oscillation-free formulation. This is called a *hierarchic displacement* formulation. Recently, Bieber et al. [21] used the idea of reparameterization to alleviate membrane locking in a curved Bernoulli beam. To obtain a more general framework, Bieber et al. [22] used a variational approach to develop the MD method. It adds extra degrees of freedom that define the strains via a carefully chosen differential relation. This can be interpreted as a kinematic law, but it is in general not identical with the actual kinematic law. The strains obtained via differentiation from the extra degrees of freedom are incorporated in a mixed sense. Compared to HF, the MD method can be used not only to treat transverse shear locking but also to alleviate membrane locking in curved beams and shells. In spite of its simplicity, the MD method introduces the question of how to handle certain additional constraints that are necessary to be imposed to obtain a well-posed system of equations. It is noted that the null space created by these additional degrees of freedom is similar to the one created in the hierarchic displacement formulation. Although the elimination of this null space is trivial for simple geometries [19, 20, 22], its generalization for complex geometries requires certain attention. It was also observed that the kinematic law chosen to handle membrane locking in Kirchhoff-Love shells using the MD method could also be used to cure in-plane shear locking in solid mechanics. Mitigation of the shear locking effects in solid mechanics is indeed the main focus of this paper.

This contribution is outlined as follows: Section 2 covers the theoretical aspects of the MD method. It provides the general framework for the method itself, which is then followed by a specific formulation to treat shear locking in solid mechanics. Furthermore, it also comments on the handling of the additional constraints needed. Section 3 demonstrates the performance of the proposed method via certain numerical examples. Here, the examples are examined in the context of FEM and IGA. Section 4 then provides some concluding remarks and hints toward possible future work.

2 | THEORETICAL ASPECTS

2.1 | General framework

The framework for the MD method is adapted from ref. [22]. The MD method starts from the Hellinger-Reissner (HR) principle with the functional

$$\Pi_{\mathrm{HR}}(\mathbf{u},\mathbf{S}) = \underbrace{\int_{\Omega} \left(\frac{1}{2}\mathbf{S}^{\mathrm{T}}\mathbf{C}^{-1}\mathbf{S} - \mathbf{E}_{\mathrm{u}}^{\mathrm{T}}\mathbf{S}\right) \mathrm{d}\Omega}_{\Pi_{\mathrm{HR}}^{\mathrm{int}}} + \underbrace{\int_{\Omega} \mathbf{u}^{\mathrm{T}}\mathbf{b}\,\mathrm{d}\Omega + \int_{\Gamma_{\sigma}} \mathbf{u}^{\mathrm{T}}\hat{\mathbf{t}}\,\mathrm{d}\Gamma_{\sigma}}_{\Pi_{\mathrm{HR}}^{\mathrm{ext}}} \rightarrow \mathrm{stat.} \tag{1}$$

Here, $\mathbf{u}$ denotes the displacement vector, and $\mathbf{S}$, $\mathbf{C}$, and $\mathbf{E}_\mathrm{u}$ denote the second Piola-Kirchhoff stress tensor, the material tensor, and the Green-Lagrange strain tensor, respectively. Furthermore, $\mathbf{b}$ and $\hat{\mathbf{t}}$ are the body forces on the domain Ω and traction forces on the Neumann boundary Γ_σ, respectively. The subscript $(\cdot)_\mathrm{u}$ indicates that $(\cdot)$ is computed from $\mathbf{u}$ via the nonlinear differential operator $\mathcal{L}(\mathbf{u})$ from the underlying kinematic law. For example, the Green-Lagrange strains are computed using

$$\mathbf{E}_\mathrm{u} = \mathcal{L}(\mathbf{u})\mathbf{u}. \tag{2}$$

Assuming a linear material law, the second Piola-Kirchhoff stress tensor can be written as

$$\mathbf{S} = \mathbf{C}\mathbf{E}, \tag{3}$$

where $\mathbf{E}$, for the time being, is an independent strain field. This gives rise to the modified Hellinger-Reissner functional

$$\Pi_\mathrm{HR}(\mathbf{u}, \mathbf{E}) = \int_\Omega \left(\frac{1}{2}\mathbf{E}^\mathrm{T}\mathbf{C}\mathbf{E} - \mathbf{E}_\mathrm{u}^\mathrm{T}\mathbf{C}\mathbf{E} \right) \mathrm{d}\Omega + \int_\Omega \mathbf{u}^\mathrm{T}\mathbf{b}\,\mathrm{d}\Omega + \int_{\Gamma_\sigma} \mathbf{u}^\mathrm{T}\hat{\mathbf{t}}\,\mathrm{d}\Gamma_\sigma \to \mathrm{stat}. \tag{4}$$

It was observed in ref. [22] that discretization based on this functional can still lead to oscillations in the stress resultants, depending on the chosen ansatz spaces for $\mathbf{u}$ and $\mathbf{E}$. In particular, it is in general not possible to define appropriate shape functions to avoid locking while at the same time respecting the paradigm of using equal-order interpolation of all fields. Locking effects may be reintroduced by choosing certain approximations that can recreate function spaces for all the fields similar to the standard displacement (or primal) formulation based on the virtual work principle. Thus, the method is bound by the *limitation principle* [23, 24].

The basic idea of the MD method is therefore to construct a strain field that is derived from additional degrees of freedom $\bar{\mathbf{u}}$ according to a particular differential relation, expressed by the operator $\bar{\mathcal{L}}$, which is in general not identical to the usual kinematic law,

$$\mathbf{E} =: \mathbf{E}_{\bar{\mathrm{u}}} = \bar{\mathcal{L}}\bar{\mathbf{u}}. \tag{5}$$

The subscript $(\cdot)_{\bar{\mathrm{u}}}$ indicates that $(\cdot)$ is computed via the newly introduced variable $\bar{\mathbf{u}}$. The differentiation ensures the achievement of suitable lower-order spaces for the strain components, thereby allowing the method to be locking-free when using equal-order interpolation for all unknown fields, that is, $\mathbf{u}$ and $\bar{\mathbf{u}}$. Introducing Equation (2) into (4) results in

$$\Pi_\mathrm{HR}(\mathbf{u}, \bar{\mathbf{u}}) = \int_\Omega \left(\frac{1}{2}\mathbf{E}_{\bar{\mathrm{u}}}^\mathrm{T}\mathbf{C}\mathbf{E}_{\bar{\mathrm{u}}} - \mathbf{E}_\mathrm{u}^\mathrm{T}\mathbf{C}\mathbf{E}_{\bar{\mathrm{u}}} \right) \mathrm{d}\Omega + \int_\Omega \mathbf{u}^\mathrm{T}\mathbf{b}\,\mathrm{d}\Omega + \int_{\Gamma_\sigma} \mathbf{u}^\mathrm{T}\hat{\mathbf{t}}\,\mathrm{d}\Gamma_\sigma \to \mathrm{stat}. \tag{6}$$

Since the derivatives of $\bar{\mathbf{u}}$ via $\bar{\mathcal{L}}$ result in strains, $\bar{\mathbf{u}}$ itself can be identified as a a *displacement-like* variable. It is to be noted that the actual displacements are still $\mathbf{u}$, whereas $\bar{\mathbf{u}}$ is only used for the computation of the strain field. Next, we write all the unknown quantities in a single vector $\tilde{\mathbf{u}}$,

$$\tilde{\mathbf{u}} = \begin{bmatrix} \mathbf{u} \\ \bar{\mathbf{u}} \end{bmatrix}. \tag{7}$$

For the tangent matrix of the discretized system, variation and linearization of the internal part of the functional is needed, providing

$$\delta\Pi_{\mathrm{HR},\tilde{\mathbf{u}}}^\mathrm{int} = \int_\Omega (\delta\mathbf{E}_{\bar{\mathrm{u}}}^\mathrm{T}\mathbf{C}\mathbf{E}_{\bar{\mathrm{u}},\tilde{\mathbf{u}}} - \delta\mathbf{E}_{\mathrm{u},\tilde{\mathbf{u}}}^\mathrm{T}\mathbf{C}\mathbf{E}_{\bar{\mathrm{u}}} - \delta\mathbf{E}_\mathrm{u}^\mathrm{T}\mathbf{C}\mathbf{E}_{\bar{\mathrm{u}},\tilde{\mathbf{u}}} - \mathbf{E}_{\mathrm{u},\tilde{\mathbf{u}}}^\mathrm{T}\mathbf{C}\delta\mathbf{E}_{\bar{\mathrm{u}}})\,\mathrm{d}\Omega. \tag{8}$$

Here, $(\cdot)_{,\tilde{\mathbf{u}}}$ denotes the partial derivative of $(\cdot)$ with respect to the total vector of degrees of freedom $\tilde{\mathbf{u}}$. As the differential operator $\bar{\mathcal{L}}$ is linear by construction, the term containing $\delta\mathbf{E}_{\bar{\mathrm{u}},\tilde{\mathbf{u}}}$ that would technically show up in Equation (8) is zero. For geometrically linear problems, also the second term in the integrand vanishes.

2.2 | Formulation for problems in 2D linear elasticity

This section will focus on the definition of the differential operator $\bar{\mathcal{L}}$ and the vector $\bar{\mathbf{u}}$ to alleviate shear locking problems in linear elasticity. They are defined here for the 2D case, but their extension to the 3D case should be simple and straightforward. Without loss of generality, the expressions in this section are written in accordance with linear kinematics. However, they can be directly applied to geometrically nonlinear problems. So, Equation (2) with linear kinematics assuming a plane stress case is written as

$$\mathbf{E}_{\mathrm{u}} \approxeq \boldsymbol{\varepsilon}_{\mathrm{u}} = \begin{bmatrix} \varepsilon_{xx} \\ \varepsilon_{yy} \\ 2\varepsilon_{xy} \end{bmatrix} = \underbrace{\begin{bmatrix} \frac{\partial}{\partial x} & 0 \\ 0 & \frac{\partial}{\partial y} \\ \frac{\partial}{\partial y} & \frac{\partial}{\partial x} \end{bmatrix}}_{\mathcal{L}} \underbrace{\begin{bmatrix} u_x \\ u_y \end{bmatrix}}_{\mathbf{u}}, \tag{9}$$

where the physical domain Ω lies in the x-y plane, and u_x and u_y denote the horizontal and the vertical displacements. Moreover, $\boldsymbol{\varepsilon}_{\mathrm{u}}$ denotes the linearized strain. The corresponding linearized stress tensor is denoted by $\boldsymbol{\sigma}_{\mathrm{u}}$. In FEM, for linear quadrilateral elements (Q1), it is well known that in-plane bending modes are accompanied by non-zero shear strains that trigger shear locking. The origin of shear locking can be explained in a simple manner by considering a Q1 element for which the local coordinates ξ and η are identical to the global coordinates, x and y. This means that the ansatz spaces for the displacements can be spanned by functions of the form $\{u_x, u_y\} \in \mathrm{span}\{1, x, y, xy\}$ and, according to Equation (9), we have

$$\varepsilon_{xx} \in \mathrm{span}\{1, y\}, \tag{10a}$$

$$\varepsilon_{yy} \in \mathrm{span}\{1, x\}, \tag{10b}$$

$$\varepsilon_{xy} \in \mathrm{span}\{1, x, y\}. \tag{10c}$$

The in-plane bending modes $u_x = xy$ and $u_y = xy$ are connected with the linear terms in ε_{xx} and ε_{yy}, which are related to bending normal strains and stresses. However, they also trigger the linear components in ε_{xy}. As these are not desired for the case of pure "bending", they are considered as parasitic shear terms. Indeed, they give rise to non-physical, additional stiffness and oscillating shear strains and stresses. If the shear strains are modified such that the linear terms in Equation (10c) vanish, shear locking is removed. This can be achieved by modifying the kinematic equation for the shear part in the context of the MD method by defining

$$\mathbf{E}_{\bar{\mathrm{u}}} \approxeq \boldsymbol{\varepsilon}_{\bar{\mathrm{u}}} = \begin{bmatrix} \varepsilon_{xx} \\ \varepsilon_{yy} \\ 2\varepsilon_{xy} \end{bmatrix} = \underbrace{\begin{bmatrix} \frac{\partial}{\partial x} & 0 & 0 \\ 0 & \frac{\partial}{\partial y} & 0 \\ 0 & 0 & \frac{\partial^2}{\partial x \partial y} \end{bmatrix}}_{\bar{\mathcal{L}}} \underbrace{\begin{bmatrix} \bar{u}_x \\ \bar{u}_y \\ \bar{u}_{xy} \end{bmatrix}}_{\bar{\mathbf{u}}}, \tag{11}$$

Thus, the strain vector $\boldsymbol{\varepsilon}_{\bar{\mathrm{u}}}$ is obtained from the additional degrees of freedom $\bar{\mathbf{u}}$ via the differential operator $\bar{\mathcal{L}}$. If the latter was identical to $\mathcal{L}$, representing the standard kinematic equations, introducing Equation (11) into the functional (6) would provide finite elements that are equivalent to those obtained with a standard displacement formulation. Indeed, the expressions in Equation (11) relating to normal strains are the same as in the kinematic Equation (9) and thus the normal strains remain unchanged. For the shear strains, however, a new expression is introduced via the MD method.

In an actual implementation, it is therefore convenient to simply compute the normal strain part from a standard displacement formulation and only explicitly introduce the third row of Equation (11) as a scalar equation,

$$\mathbf{E}_{\bar{\mathrm{u}}} \approxeq \boldsymbol{\varepsilon}_{\bar{\mathrm{u}}} =: \varepsilon_{\bar{u}} = \underbrace{\begin{bmatrix} \frac{\partial^2}{\partial x \partial y} \end{bmatrix}}_{\bar{\mathcal{L}}} \underbrace{\begin{bmatrix} \bar{u}_{xy} \end{bmatrix}}_{\bar{\mathbf{u}}}, \tag{12}$$

which is then used to construct the shear part of the element formulation using a modified functional in the form of Equation (6) that only contains the shear strains.

The newly introduced variable $\bar{u}_{xy}$ has a unit of "displacement squared" due to the involvement of a second derivative, which is similar to the variable introduced in ref. [22] to treat membrane locking in Kirchhoff-Love shells. From numerical evidence, it was observed that the continuity requirement of such a formulation is not modified, even though a second derivative is involved, which is not usually the case in standard FEM. Furthermore, the presence of the second derivative causes only the shear strains to jump across element boundaries, which is also the case in standard FEM. In all numerical experiments, applying C^0-continuous shape functions for all variables did not cause any artificial instabilities. Nevertheless, further theoretical and mathematical analysis on this subject is required.

Up to here, in order to explain the basic concept, it was assumed that the physical and the parametric coordinate systems are identical, that is, $x = \xi$ and $y = \eta$. However, in general, this is not applicable. In particular, for distorted elements, nonlinear terms in ξ and η are obtained while computing the second derivatives with respect to the global coordinates x and y. These originate from the transformation matrices used to map the derivatives between the different coordinate systems. This issue is revisited shortly in Section 3.2. As a result, the patch test for constant shear strains fails for distorted meshes. Defining the operator $\bar{\mathcal{L}}$ with derivatives in the parametric space circumvents the need for coordinate transformation and thus guarantees passing the patch test. Thus, we redefine $\varepsilon_{\bar{u}}$ in Equation (12) as

$$\varepsilon_{\bar{u}} = \underbrace{\left[\frac{\partial^2}{\partial\xi\partial\eta}\right]}_{\bar{\mathcal{L}}} \underbrace{\left[\bar{u}_{\xi\eta}\right]}_{\bar{\mathbf{u}}}. \tag{13}$$

The crucial property of the construction of $\bar{\mathcal{L}}$ in Equation (13) is that the mixed second derivative effectively removes the linear terms in Equation (10c), which makes the formulation shear-locking-free. Working in the parametric space to alleviate locking is also a well-known methodology, for example, in the EAS method. The chosen $\bar{\mathcal{L}}$ in Equation (13) thus serves as an operator that removes the parasitic shear terms in the parametric space. Note that $\bar{u}_{\xi\eta}$—as opposed to $\bar{u}_{xy}$—is a dimensionless quantity. The subscripts $(\cdot)_{xy}$ and $(\cdot)_{\xi\eta}$ in Equation (12) and Equation (13), respectively, are here used to denote the coordinate system where the derivatives were computed. However, they both are global quantities residing at the nodes and are interpolated using the same function spaces adopted for $\mathbf{u}$.

Although the particular construction of the MD method was motivated by Equation (10) in the context of a Q1 element, the construction of $\bar{\mathcal{L}}$ according to Equation (13) is applicable for higher-order function spaces, independent of the discretization scheme, as it creates the necessary lower-order spaces needed to alleviate shear locking *prior* to discretization.

2.3 | Additional constraints

It was already stated in ref. [22] that certain constraints are to be defined for the MD method in order to avoid spurious modes associated with the degrees of freedom $\bar{\mathbf{u}}$. These can be enforced, for instance, through Lagrange multipliers or a penalty method. In this section, the constraints are defined for the MD method in the context of linear elasticity, and they are enforced via a penalty approach. At first, we identify the source of the zero-energy modes. The integral of Equation (13) with respect to ξ and η can be written as

$$\bar{u}_{\xi\eta} = \int_{\xi}\int_{\eta} \varepsilon_{\bar{u}}\, \mathrm{d}\eta\, \mathrm{d}\xi + F(\xi) + G(\eta), \tag{14}$$

with $F(\xi)$ and $G(\eta)$ representing the integration constants for integration in η- and ξ-direction, respectively. They are arbitrary functions of ξ and η that do not have an effect on the value of the strain $\varepsilon_{\bar{u}}$. Thus, the solution for $\bar{u}_{\xi\eta}$ is not unique, giving rise to a non-zero kernel (null space) of the tangent matrix. The modes $\bar{u}_{\xi\eta} = F(\xi)$ and $\bar{u}_{\xi\eta} = G(\eta)$ are the zero-energy modes that have to be suppressed.

In ref. [22], similar modes were suppressed by enforcing certain Dirichlet boundary conditions on $\bar{\mathbf{u}}$ for specific examples in the context of plates and shells. This method is briefly explained in the following. Let us consider, for example, the zero-energy mode $\bar{u}_{\xi\eta} = G(\eta)$ depicted on a unit square with two different meshes constructed using Q1 elements; see Figure 1. Even though the integration in Equation (14) is performed on an element level, in Figure 1, for illustrative purposes, this

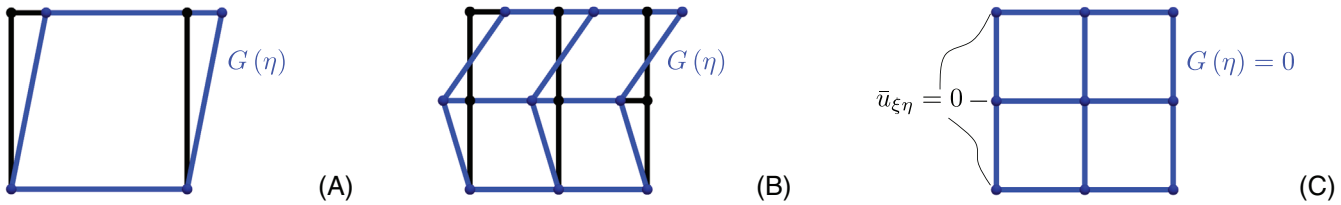

FIGURE 1 Zero-energy mode $\bar{u}_{\xi\eta} = G(\eta)$ depicted for (A) 1×1 mesh and (B) 2×2 mesh; (C) Constraint on $\bar{u}_{\xi\eta}$ to suppress the mode $G(\eta)$..

distinction is explicitly avoided, and we show the global function $\bar{u}_{\xi\eta} = G(\eta)$, obtained after assembly, when more than one element is involved. Furthermore, for convenience here, we express everything in terms of ξ and η, but it should be clear that the zero-energy modes to be suppressed are always to be thought of on a system level. For structured meshes, the rank of the stiffness matrix obtained will be proportional to the number of nodes in the vertical direction along an edge. This is seen in Figure 1A,B, where the number of independent zero-energy modes at different positions along the vertical direction increases from two to three when the number of nodes increases from two to three along an edge in this direction. This would imply that if we constrain the degree of freedom $\bar{u}_{\xi\eta}$ at every node along the η-direction (see Figure 1C), the mode $G(\eta)$ is suppressed because the mode is constant along the ξ-direction. Similar argumentation holds to suppress the mode $F(\xi)$ along the other edge of the square domain. This way of suppressing the zero-energy modes works well for simple geometries with structured meshes [19, 20, 22]. For unstructured and distorted meshes as well as complex domains, identifying the locations to be fixed from the available knowledge of the zero-energy modes of the system is a tedious task and can also result in an over-constrained system.

This encourages us to find an alternative way to get rid of the artificial zero-energy modes. Since the information about the zero-energy modes is known a priori, as they are an outcome of the chosen $\bar{\mathcal{L}}$, we can define a new tensor $\mathbf{E}_\mathrm{p}$, which relates to the vector $\bar{\mathbf{u}}$ via a carefully chosen differential operator $\mathcal{L}_\mathrm{p}$ that provides non-zero contributions from the spurious modes $F(\xi)$ and $G(\eta)$,

$$\mathbf{E}_\mathrm{p} = \mathcal{L}_\mathrm{p}\bar{\mathbf{u}}. \tag{15}$$

We then add this to the functional in Equation (6) in the form of a penalty term to get

$$\Pi_\mathrm{HR}(\mathbf{u}, \bar{\mathbf{u}}) = \int_\Omega \left(\frac{1}{2}\mathbf{E}_{\bar{\mathbf{u}}}^\mathrm{T}\mathbf{C}\mathbf{E}_{\bar{\mathbf{u}}} - \mathbf{E}_\mathbf{u}^\mathrm{T}\mathbf{C}\mathbf{E}_{\bar{\mathbf{u}}} + \frac{1}{2}\epsilon_\mathrm{p}\mathbf{E}_\mathrm{p}^\mathrm{T}\mathbf{C}\mathbf{E}_\mathrm{p} \right) \mathrm{d}\Omega + \int_\Omega \mathbf{u}^\mathrm{T}\mathbf{b}\,\mathrm{d}\Omega + \int_{\Gamma_\sigma} \mathbf{u}^\mathrm{T}\hat{\mathbf{t}}\,\mathrm{d}\Gamma_\sigma \to \mathrm{stat}. \tag{16}$$

Here, ϵ_p is a small number that is chosen such that $0 < \frac{1}{2}\epsilon_\mathrm{p}\mathbf{E}_\mathrm{p}^\mathrm{T}\mathbf{C}\mathbf{E}_\mathrm{p} \ll \frac{1}{2}\mathbf{E}_{\bar{\mathbf{u}}}^\mathrm{T}\mathbf{C}\mathbf{E}_{\bar{\mathbf{u}}} - \mathbf{E}_\mathbf{u}^\mathrm{T}\mathbf{C}\mathbf{E}_{\bar{\mathbf{u}}}$. The effect of this penalty factor ϵ_p on the solution of the system of equations is discussed briefly in Section 3.2. The penalty term is scaled with the material tensor to be consistent with the units. The inclusion of this penalty term also adds a term $\delta\Pi^\mathrm{int}_{\mathrm{HR,p},\tilde{\mathbf{u}}}$ to Equation (8) in the computation of the tangent stiffness matrix and is given by

$$\delta\Pi^\mathrm{int}_{\mathrm{HR,p},\tilde{\mathbf{u}}} = \int_\Omega (\epsilon_\mathrm{p}\delta\mathbf{E}^\mathrm{T}_{\mathrm{p},\tilde{\mathbf{u}}}\mathbf{C}\mathbf{E}_\mathrm{p})\,\mathrm{d}\Omega. \tag{17}$$

This imposes the constraints in a weak sense, while the approach from ref. [22] enforces the required Dirichlet boundary conditions in a strong sense. For the general case, for the chosen $\bar{\mathcal{L}}$ in Equation (13), the zero-energy modes are linear functions in ξ and η, including constants. It is therefore sensible to impose a constraint on the first derivatives of $\bar{u}_{\xi\eta}$ with respect to ξ and η by defining

$$\mathbf{E}_{\mathrm{p}_\xi} \approxeq \boldsymbol{\varepsilon}_{\mathrm{p}_\xi} =: \varepsilon_{\mathrm{p}_\xi} = \underbrace{\left[\frac{\partial}{\partial\xi}\right]}_{\mathcal{L}_{\mathrm{p}_\xi}} \bar{u}_{\xi\eta}, \tag{18a}$$

$$\mathbf{E}_{\mathrm{p}_\eta} \approxeq \boldsymbol{\varepsilon}_{\mathrm{p}_\eta} =: \varepsilon_{\mathrm{p}_\eta} = \underbrace{\left[\frac{\partial}{\partial\eta}\right]}_{\mathcal{L}_{\mathrm{p}_\eta}} \bar{u}_{\xi\eta}, \tag{18b}$$

thereby eliminating the linear terms. The constant terms can then be eliminated by applying discrete Dirichlet boundary conditions. Due to the involvement of a second derivative, two constraints are to be enforced here, and hence Equation (16) can be rewritten as

$$\Pi_{\mathrm{HR}}(\mathbf{u},\bar{\mathbf{u}}) = \int_\Omega \left(\frac{1}{2}\mathbf{E}_{\bar{\mathrm{u}}}^{\mathrm{T}}\mathbf{C}\mathbf{E}_{\bar{\mathrm{u}}} - \mathbf{E}_{\mathrm{u}}^{\mathrm{T}}\mathbf{C}\mathbf{E}_{\bar{\mathrm{u}}} + \frac{1}{2}\epsilon_{\mathrm{p}}\mathbf{E}_{\mathrm{p}_\xi}^{\mathrm{T}}\mathbf{C}\mathbf{E}_{\mathrm{p}_\xi} + \frac{1}{2}\epsilon_{\mathrm{p}}\mathbf{E}_{\mathrm{p}_\eta}^{\mathrm{T}}\mathbf{C}\mathbf{E}_{\mathrm{p}_\eta} \right) \mathrm{d}\Omega + \int_\Omega \mathbf{u}^{\mathrm{T}}\mathbf{b}\,\mathrm{d}\Omega + \int_{\Gamma_\sigma} \mathbf{u}^{\mathrm{T}}\hat{\mathbf{t}}\,\mathrm{d}\Gamma_\sigma \rightarrow \mathrm{stat.} \tag{19}$$

This then modifies the computation of the tangent stiffness matrix, similar to Equation (17), but it is not explicitly expressed here again. In theory, different penalty parameters can be chosen for $\epsilon_{\mathrm{p}_\xi}$ and $\epsilon_{\mathrm{p}_\eta}$. Here, however, a single parameter ϵ_{p} is used. This strategy is adopted for all the numerical examples in Section 3. A similar methodology can be easily extrapolated to handle the constraints in the context of plates and shells for the hierarchic displacement formulation [19, 20] and the MD method [22].

3 | NUMERICAL EXAMPLES

3.1 | Overview

Four different numerical examples are considered to study the performance of the developed formulation. The first one is a *patch test* in Section 3.2 as a numerical consistency test for the MD method. Second, the popular *Cook's membrane* [25] problem is adopted in Section 3.3 to study the element's behavior with respect to shear locking. The *bending of a curved beam* example from ref. [10] is then investigated in Section 3.4 to study the element's behavior in the context of trapezoidal locking. Finally, the *coiling of a straight beam* example inspired by refs. [26, 27] is analyzed for signs of geometrically nonlinear locking effects in Section 3.5. Nonlinear locking is a phenomenon triggered by the use of a higher number of integration points [26–28]. All simulations were performed using the open-source C++ library Ikarus [29]. Unless otherwise indicated, isotropic linear elastic material law is used for all the examples.

The following abbreviations are used in the following:

- **Q1**: Standard bilinear quadrilateral element.
- **Q1E4**: Q1 element enhanced with four EAS parameters according to refs. [7, 8]. The implementation aspects of the nonlinear EAS formulation are adapted from refs. [30] and [31].
- **Q1MD**: Q1 element where the shear strains are modified according to the MD method via Equation (13). The penalty approach is used to suppress the zero-energy modes via Equation (18). For all examples, $\bar{u}_{xy} = 0$ at the origin, that is, $\bar{u}_{xy}(0,0) = 0$ unless stated otherwise.
- **BFE**: Isogeometric finite elements with B-splines as basis functions, based on a standard displacement formulation using the kinematic equations in Equation (9).
- **BMD**: Isogeometric finite elements with B-splines as basis functions, based on the MD method.

The notations used for the geometrically linear problems (Sections 3.2, 3.3, and 3.4) and the geometrically nonlinear problem (Section 3.5) are the same.

3.2 | Patch test

For the patch test, the geometry definition is adapted from ref. [32]. The problem is defined in Figure 2, where nodal positions and element numbers are shown. Figure 2A depicts boundary conditions for a constant tension case, while Figure 2B represents a constant shear case. For the constant shear case, u_y is set to zero at all nodal positions. Assuming plane stress conditions, the parameters Young's modulus $E = 1000$, Poisson's ratio $\nu = 0.25$, load $F = 0.12$, and the penalty factor $\epsilon_{\mathrm{p}} = 10^{-10}$ are chosen. To pass the patch test, the expected constant stress state in all the elements is given by $\sigma_{u,xx} = 1.0, \sigma_{u,yy} = 0.0$, and $\sigma_{\bar{u},xy} = 0.0$ for the tension test and $\sigma_{u,xx} = 0.0, \sigma_{u,yy} = 0.0$, and $\sigma_{\bar{u},xy} = 0.5$ for the shear test. The proposed Q1MD element is able to exactly represent these constant stress states and therefore passes the patch test.

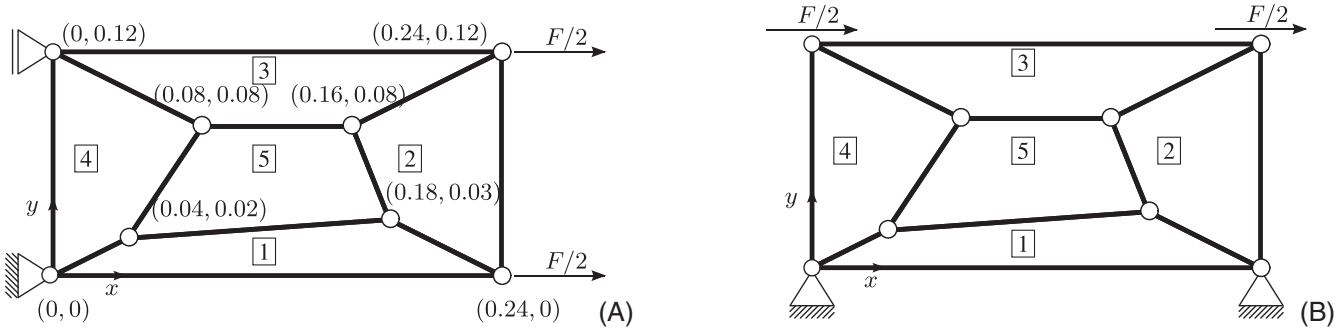

FIGURE 2 Patch test: problem description (adapted from ref. [32]): (A) constant tension case; (B) constant shear case.

As it was mentioned in Section 2.2, coordinate transformation plays a crucial role for the element to pass the patch test. Passing the patch test for normal strains is not a problem because the proposed element provides similar results to a standard Galerkin formulation in this case. It is the constant shear strain that poses challenges.

In order to illustrate this, let us consider the constant shear case and element 3 from Figure 2B. Here, $\xi \in [-1, 1]$ and $\eta \in [-1, 1]$. The relation between global cartesian and element coordinates for this element is given by

$$\begin{bmatrix} x \\ y \end{bmatrix} = \begin{bmatrix} \frac{3}{25} + \frac{(\eta+2)\xi}{25} \\ \frac{\eta}{50} + \frac{1}{10}. \end{bmatrix} \tag{20}$$

The shear stress $\sigma_{\bar{u},xy}$ obtained from the formulation using Equation (12) is

$$\sigma_{\bar{u},xy} = \frac{11250 \ln(3)}{(\eta + 2)^2(21 \ln(3)\epsilon_p - 9\epsilon_p + 10000)}. \tag{21}$$

It is nonlinear in η, obviously contradicting the expected constant stress state. Using the formulation with Equation (13) results in

$$\sigma_{\bar{u},xy} = \frac{6}{4375 \ln(3)\epsilon_p - 1875\epsilon_p + 12}, \tag{22}$$

which is a constant in ξ and η.

The Equations (21) and (22) are explicitly written in terms of ϵ_p to highlight the influence of the penalty parameter. As is typical for a penalty method, the parameter ϵ_p has a certain influence on the computational results. In Equation (22), it is observed that the correct constant shear state with $\sigma_{\bar{u},xy} = 0.5$ is only achieved if $\epsilon_p \approxeq 0$. Thus, choosing a small value for ϵ_p is important for the element to be consistent. Moreover, the choice of the penalty parameter has an influence on the conditioning of the tangent matrix. Obviously, a method to regularize the MD method that does not rely on a penalty parameter is desirable, and it is therefore subject to ongoing research.

3.3 | Cook's membrane

Cook's membrane problem is solved under the assumption of plane stress and with parameters $E = 1, \nu = 1/3, \hat{t} = 1/16$, and $\epsilon_p = 10^{-8}$. Simulations are performed considering a structured mesh and an unstructured mesh, as shown in Figure 3A,B. The vertical displacement in the top right corner A is denoted by $u_{y,A}$, and the stress component $\sigma_{u,xx}$ for the shaded element at the center of the bottom edge B is denoted by $\sigma_{u,xx,B}$. These points are also depicted in Figure 3. For convergence studies, every element edge is bisected, thereby increasing the total number of elements by a factor of four with every mesh refinement step. Figures 4A and 5A show a better convergence of Q1MD compared to Q1 owing to its shear locking-free characteristics, while the results are poorer compared to Q1E4 because Q1MD is not free from volumetric locking. Volumetric locking is prompted here due to a non-zero Poisson's ratio. This is also seen in the convergence plots corresponding to $\sigma_{u,xx,B}$ in Figures 4B and 5B, where Q1MD shows a behavior similar to Q1, while Q1E4 exhibits a better coarse-mesh accuracy.

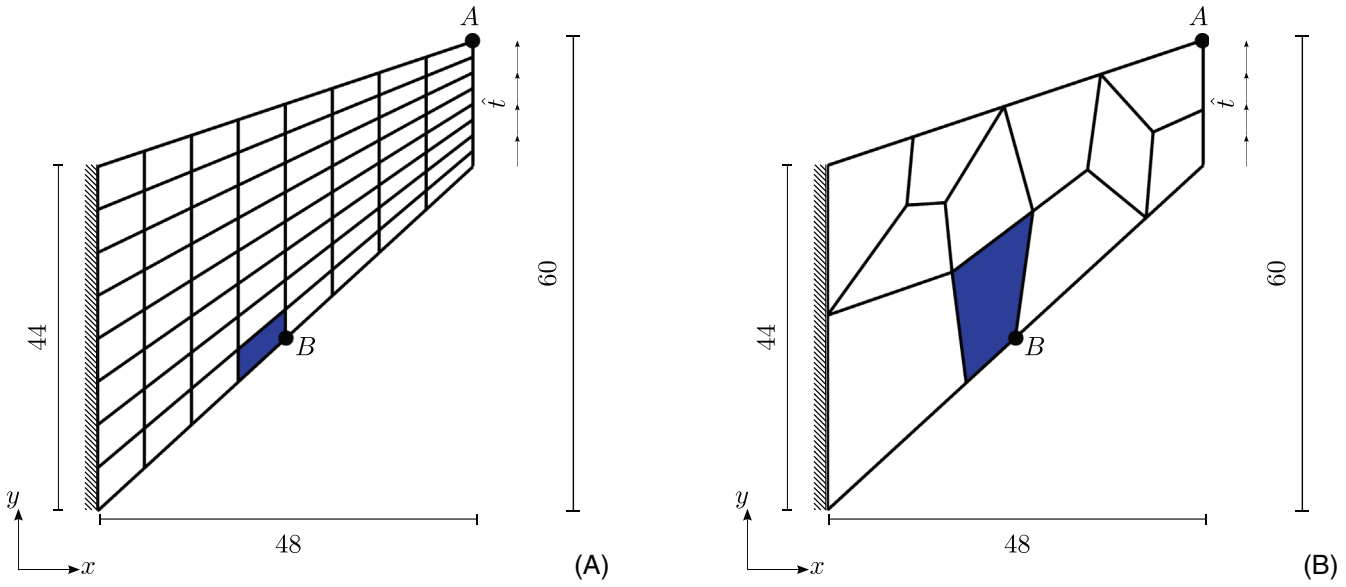

FIGURE 3 Cook's membrane problem: (A) structured mesh (adapted from ref. [25]); (B) unstructured mesh.

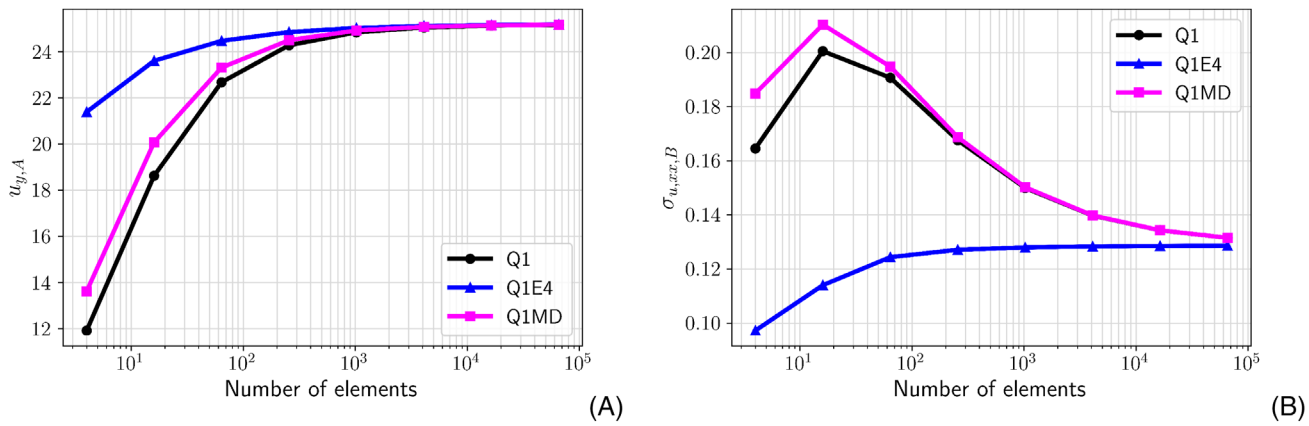

FIGURE 4 Cook's membrane example with structured mesh: (A) $u_{y,A}$ versus number of elements; (B) $\sigma_{u,xx,B}$ versus number of elements.

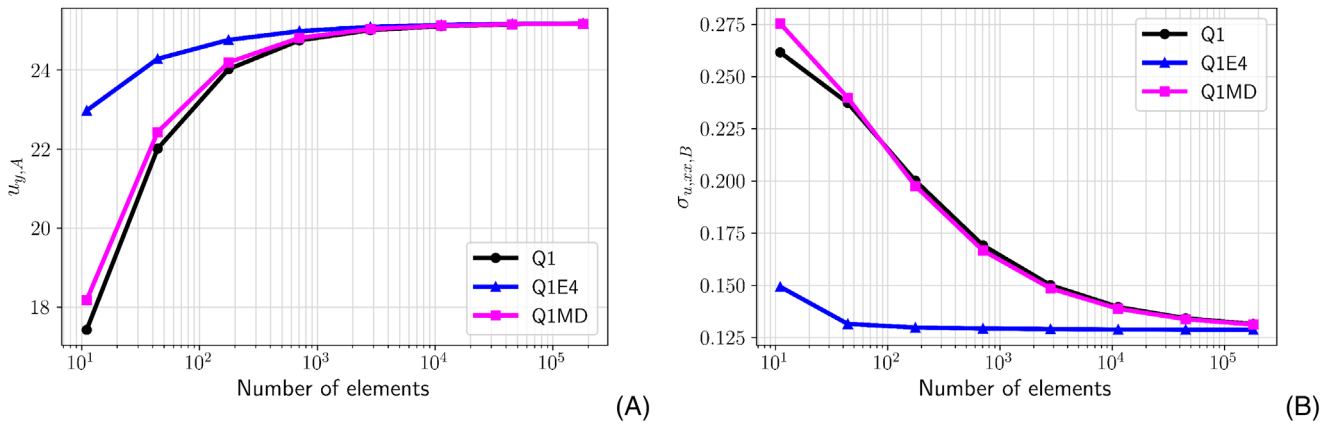

FIGURE 5 Cook's membrane example with unstructured mesh: (A) $u_{y,A}$ versus number of elements; (B) $\sigma_{u,xx,B}$ versus number of elements.

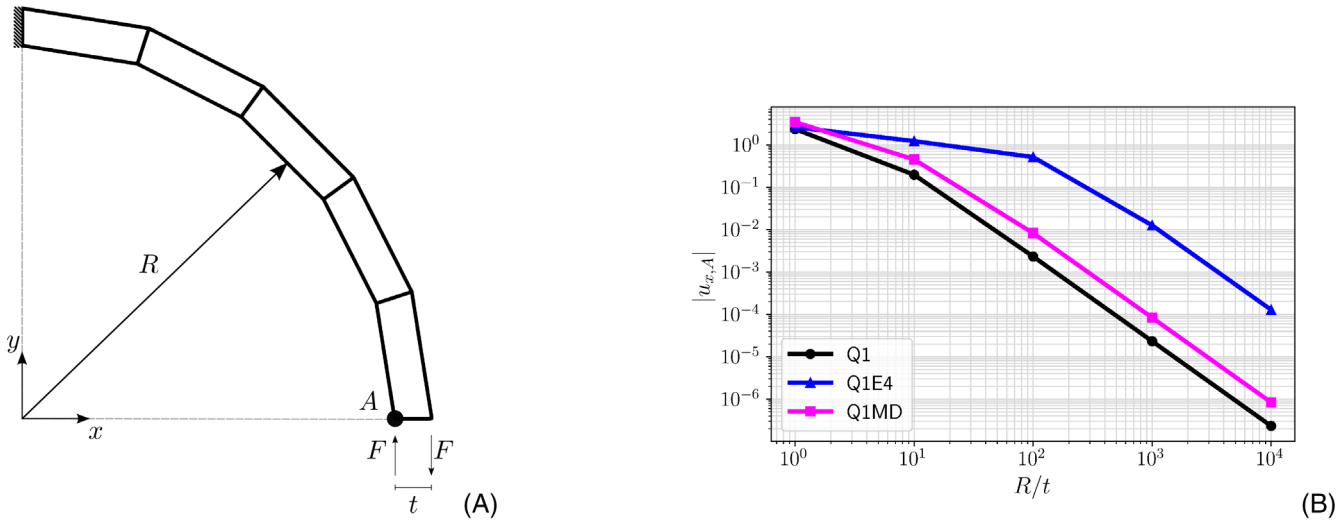

FIGURE 6 Bending of a curved beam: (A) problem description (adapted from ref. [10]); (B) $|u_{x,A}|$ versus slenderness R/t of the beam.

3.4 | Bending of a curved beam

The problem of modeling a curved beam with 2D-solid elements is illustrated in Figure 6A. Due to the initial curvature of this thin-walled structure, not only shear locking but also trapezoidal locking is expected to have a detrimental effect on the solution. Again, plane stress conditions are assumed along with parameters $E = 1000, \nu = 0, R = 10, F = t^2$, and $\epsilon_{\mathrm{p}} = 10^{-6}$. Poisson's ratio is set to zero to exclude volumetric locking. The beam is discretized with five elements. Furthermore, the constant zero-energy mode of $\bar{u}_{xy}$ is removed via the condition $\bar{u}_{xy}(0, R) = 0$. The load is proportional to t^2, such that the resulting moment is proportional to t^3, which makes the exact solution of the displacement u_x at A (see Figure 6A) independent of the thickness. Therefore, if reduced displacements are observed upon increasing the slenderness R/t, this is an indication of locking. Figure 6B shows the absolute value $|u_{x,A}|$ of the displacement at A for Q1, Q1E4, and Q1MD in dependence of the slenderness R/t. It is observed that Q1MD suffers from trapezoidal locking, similar to the standard Q1 element, because $\bar{\mathcal{L}}$ is designed to get rid of shear locking but does not address trapezoidal locking. Again, the results of Q1E4 are superior. But this time, it is not due to avoiding volumetric locking, which is excluded because Poisson's ratio is zero. The authors assume that the superior behavior is related to a lower sensitivity to distorted meshes. The same phenomenon can be observed when comparing Q1E4 to an element in which shear locking is removed by selective reduced integration of the shear strains. Nevertheless, Q1E4 is also not free from trapezoidal locking, as can be seen from the steeply descending branch after $R/t \approx 10^2$.

3.5 | Coiling of a straight beam

This problem, described in Figure 7, is solved with the parameters $E = 100, \nu = 0, L = 10$, and $\epsilon_{\mathrm{p}} = 10^{-8}$. The number of elements in the vertical direction is one ($n_{\mathrm{ele},Y} = 1$), while the number of elements in the horizontal direction ($n_{\mathrm{ele},X}$) varies, as discussed later. A St. Venant-Kirchhoff material law is used along with plane strain assumptions. The beam is coiled into a circle by prescribing a bending moment M at its tip. The analytical solution in the thin limit, according to ref. [27], for the moment to be applied to coil the beam into a full circle is given by

$$M = 2\pi \frac{E}{1-\nu^2} \frac{T^3}{12L}. \tag{23}$$

Here, T is the thickness of the beam. In a 2D setting with solid elements and a discretization with one linear element through the thickness, this moment load can be realized via a pair of forces with opposite signs and magnitude $F = M/T$ on the two nodes on the rightmost edge. These are the consistent nodal forces representing a traction load $\hat{\mathbf{t}}(\hat{s})$ applied across the element edge, as shown in Figure 7. Here, a local coordinate system $\hat{s} \in [0, 1]$ is established along the edge

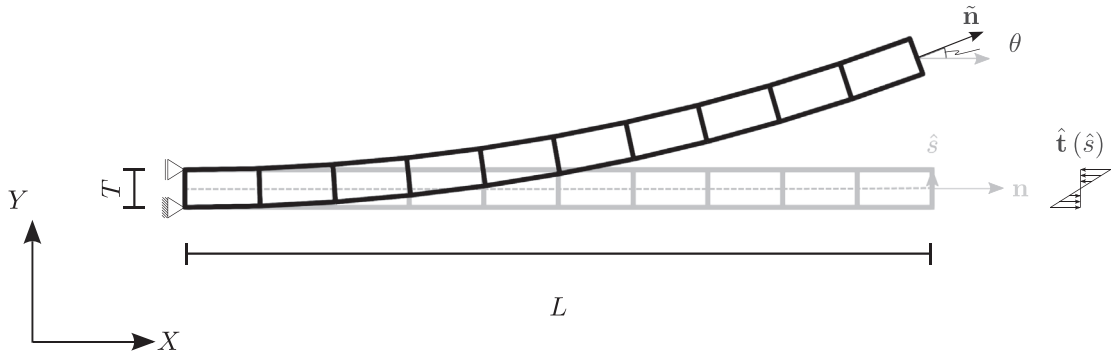

FIGURE 7 Coiling of a straight beam example: problem description (adapted from ref. [27]).

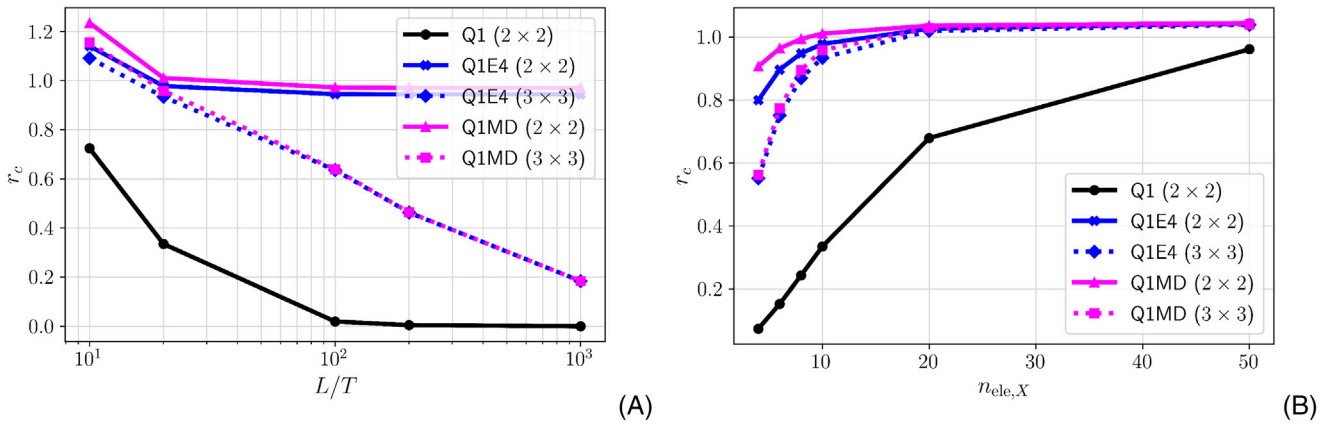

FIGURE 8 Coiling of a straight beam example: (A) r_c versus L/T ($n_{\text{ele},X} = 10$); (B) r_c versus $n_{\text{ele},X}$ ($L/T = 20$).

where the traction load is applied. The desired load state can be achieved for the chosen mesh via

$$\hat{\mathbf{t}}(\hat{s}) = (1 - 2\hat{s})\frac{6\lambda}{T}\tilde{\mathbf{n}}. \tag{24}$$

Here, λ is the load factor, $\tilde{\mathbf{n}}$ is the unit outward normal vector in the deformed configuration corresponding to the edge where the load is applied, and $\mathbf{n}$ denotes the same in the reference configuration (see Figure 7). Load control is used to perform the nonlinear analysis, where λ is incrementally increased until $\lambda = F$. Let θ denote the angle by which the normal vector $\mathbf{n}$ is rotated to reach $\tilde{\mathbf{n}}$ in the deformed state. This means that the coiling ratio $r_c = \theta/(2\pi) = 1$ when the beam is fully coiled into a circle and $r_c < 1$ indicates locking, that is, a too stiff behavior. Here, the element formulations Q1E4 and Q1MD are studied with 2×2 and 3×3 integration points. In the latter case, nonlinear locking effects are triggered. The standard displacement element Q1 is only studied with 2×2 integration points, as it is already dominated by locking effects in the linear regime. This is clearly seen in Figure 8A, where the coiling ratio tends to zero with increasing slenderness for Q1. On the other hand, the results obtained with Q1E4 and Q1MD are independent of the slenderness for 2×2 integration points. Values with $r_c > 1$ are observed for thick beams, that is, larger deformations than predicted by the analytical solution, assuming a thin beam.

When 3×3 integration points are used, both Q1E4 and Q1MD exhibit nonlinear locking effects. The values are very close to each other, as evident from Figure 8A. This is because these elements balance only the linear terms of the parasitic shear strain, while the nonlinear terms are left untouched. For Q1E4, a possible method to deal with such locking effects is discussed in detail in ref. [26]. For the Q1MD formulation, a nonlinear relationship between $\mathbf{E}_{\bar{\mathbf{u}}}$ and $\bar{\mathbf{u}}$ could be a possibility to alleviate nonlinear locking, but this idea is not discussed further in this contribution.

The mesh depicted in Figure 7 with $n_{\text{ele},X} = 10$ is chosen to study the effect of slenderness in Figure 8A. Figure 8B shows a convergence plot where r_c is plotted against $n_{\text{ele},X}$ with $L/T = 20$. Here, as expected, Q1 shows a reduced convergence rate. Q1E4 and Q1MD show similar behavior with 3×3 integration points. With 2×2 integration points, Q1MD shows better results than Q1E4 for coarser meshes. Figure 9 shows the final deformed configurations for Q1 and Q1MD for

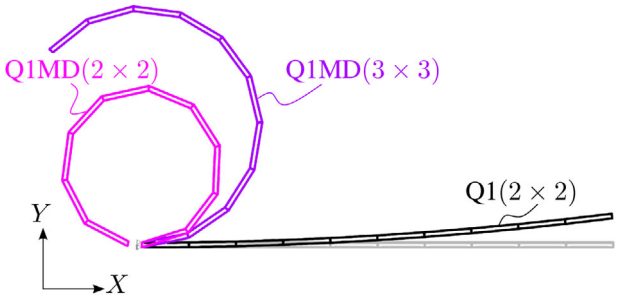

FIGURE 9 Coiling of a straight beam example: Deformed states for $L/T = 100$ (Q1E4 not shown).

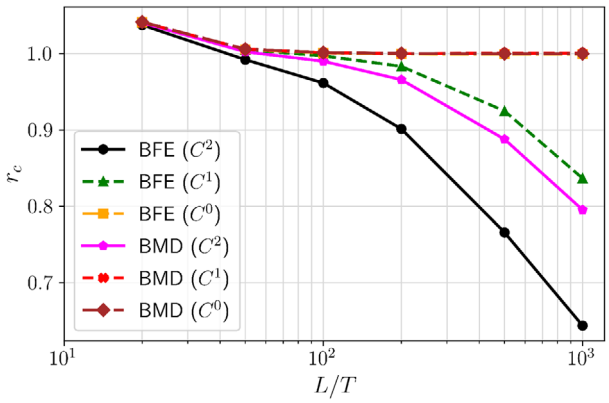

FIGURE 10 Coiling of a straight beam example with B-spline-based finite elements: r_c versus L/T.

$L/T = 100$ and different numbers of integration points. Q1E4 is not shown here as the results are similar to those of Q1MD (see Figure 8A). This also shows the unlocking feature of Q1MD with 2×2 integration points, where the beam is almost coiled into a circle, whereas both Q1MD and Q1E4 with 3×3 integration exhibit nonlinear locking, such that $r_c < 1$.

Next, the same example is investigated in the context of IGA. Using the tensor product of B-splines with cubic order in the horizontal direction ($p_\xi = 3$) and linear order in the vertical direction ($p_\eta = 1$) as shape functions, the 2D straight beam geometry is defined. Here, ξ and η denote the coordinates in the parent element space. These functions are then used to interpolate the unknown global degrees of freedom. 4×4 integration points and an 8×1 mesh are used in this case. We multiply the knots to modify the continuity between the elements in the ξ-direction. The EAS formulation is not discussed in this context. The diagram in Figure 10 shows the coiling ratio versus the slenderness of the beam for finite elements based on B-splines. Standard Galerkin elements (BFE) and mixed displacements elements (BMD) with continuities C^2, C^1, and C^0 between the elements in the horizontal direction are compared.

It is already known that if an element suffers from locking, the constraints from higher continuity between elements will further increase the stiffness. This is noticeable in Figure 10, where C^2- and C^1-continuous BFE elements show a decreasing coiling ratio with increasing slenderness. C^0-continuous BFE elements yield better approximations. C^1- and C^0-continuous BMD elements also show locking-free properties, while with C^2-continuity, the result deteriorates with increasing slenderness. This stems from the fact that more integration points are used in the vertical direction than required, as it is approximated only with linear functions, thereby causing nonlinear locking.

4 | CONCLUSIONS AND OUTLOOK

The developed MD formulation exhibits shear-locking-free characteristics for geometrically linear problems in elasticity. It is locking-free on a theoretical level, thereby facilitating its immediate application to arbitrary discretization schemes while using equal-order interpolation of all fields. Additional constraints, required to ensure well-posedness, were treated via the penalty approach, which makes their generalization convenient. However, the influence of the penalty factor ϵ_p

requires further investigation, as discussed in Section 3.2. In particular, one can study how this parameter evolves with respect to mesh distortions and how the shear modes vary with varying ϵ_p. Alternatively, it is also possible to look into other methods to enforce the constraints included in the operator $\mathcal{L}_p$. Several numerical examples were presented to investigate the performance of the developed method. Even though the formulation is shear-locking-free in the linear regime, it is still prone to volumetric, trapezoidal, and nonlinear locking effects. Fashioning an operator $\bar{\mathcal{L}}$ that can also alleviate these locking effects will be another prospect of this work. Furthermore, owing to the similarities with the EAS element in the nonlinear regime, it is anticipated that the presented MD formulation can also exhibit some well-known problems of the EAS method, for instance, the presence of artificial instabilities (hourglassing). A systematic investigation on the presence of artificial instabilities, as done for instance in ref. [26, 27], will also be a part of the future work. Finally, as there is no requirement to invert the material tensor in Equation (6), in contrast to Equation (1), the MD method is expected to be easily applicable for different constitutive laws.

ACKNOWLEDGMENTS

This project is supported by the Deutsche Forschungsgemeinschaft (DFG) under grant number BI 722/12-1. This support is gratefully acknowledged.

Open access funding enabled and organized by Projekt DEAL.

ORCID

Tarun Kumar Mitruka *Vinod Kumar Mitruka* https://orcid.org/0000-0003-0453-5347
Manfred Bischoff https://orcid.org/0000-0003-1538-4281

REFERENCES

1. Pawsey, S. F., & Clough, R. W. (1971). Improved numerical integration of thick shell finite elements. *International Journal for Numerical Methods in Engineering*, *3*(4), 575–586.
2. Hughes, T. J., Cohen, M., & Haroun, M. (1978). Reduced and selective integration techniques in the finite element analysis of plates. *Nuclear Engineering and Design*, *46*, 203–222.
3. Zienkiewicz, O. C., Taylor, R. L., & Too, J. M. (1971). Reduced integration technique in general analysis of plates and shells. *International Journal for Numerical Methods in Engineering*, *3*(2), 275–290.
4. Hughes, T. J. R. (1980). Generalization of selective integration procedures to anisotropic and nonlinear media. *International Journal for Numerical Methods in Engineering*, *15*(9), 1413–1418.
5. Hughes, T. J. R., & Tezduyar, T. E. (1981). Finite elements based upon Mindlin plate theory with particular reference to the four-node bilinear isoparametric element. *Journal of Applied Mechanics*, *48*(3), 587–596.
6. Dvorkin, E. N., & Bathe, K. J. (1984). A continuum mechanics based four-node shell element for general non-linear analysis. *Engineering and Computational*, *1*(1), 77–88.
7. Simo, J. C., & Rifai, M. S. (1990). A class of mixed assumed strain methods and the method of incompatible modes. *International Journal for Numerical Methods in Engineering*, *29*(8), 1595–1638.
8. Andelfinger, U., & Ramm, E. (1993). EAS-elements for two-dimensional, three-dimensional, plate and shell structures and their equivalence to HR-elements. *International Journal for Numerical Methods in Engineering*, *36*(8), 1311–1337.
9. Bletzinger, K. U., Bischoff, M., & Ramm, E. (2000). A unified approach for shear-locking-free triangular and rectangular shell finite elements. *Computers and Structures*, *75*(3), 321–334.
10. Bischoff, M., Koschnick, F., & Bletzinger, K. U. (2003). Stabilized DSG Elements – A New Paradigm in Finite Element Technology. In: Proceedings 4th European LS-DYNA Users Conference, Implicit / New Developments, Germany, 49–62.
11. Hughes, T., Cottrell, J., & Bazilevs, Y. (2005). Isogeometric analysis: CAD, finite elements, NURBS, exact geometry and mesh refinement. *Computer Methods in Applied Mechanics and Engineering*, *194*(39–41), 4135–4195.
12. Adam, C., Bouabdallah, S., Zarroug, M., & Maitournam, H. (2014). Improved numerical integration for locking treatment in isogeometric structural elements, Part I: Beams. *Computer Methods in Applied Mechanics and Engineering*, *279*, 1–28.
13. Adam, C., Hughes, T., Bouabdallah, S., Zarroug, M., & Maitournam, H. (2015). Selective and reduced numerical integrations for NURBS-based isogeometric analysis. *Computer Methods in Applied Mechanics and Engineering*, *284*, 732–761.
14. Elguedj, T., Bazilevs, Y., Calo, V., & Hughes, T. (2008). B-bar and F-bar projection methods for nearly incompressible linear and non-linear elasticity and plasticity using higher-order NURBS elements. *Computer Methods in Applied Mechanics and Engineering*, *197*(33–40), 2732–2762.
15. Caseiro, J. F., Valente, R. A. F., Reali, A., Kiendl, J., Auricchio, F., & Alves De Sousa, R. J. (2014). On the assumed natural strain method to alleviate locking in solid-shell NURBS-based finite elements. *Computational Mechanics*, *53*, 1341–1353.
16. Cardoso, R. P. R., & Cesar De Sa, J. M. A. (2012). The enhanced assumed strain method for the isogeometric analysis of nearly incompressible deformation of solids. *International Journal for Numerical Methods in Engineering*, *92*(1), 56–78.
17. Echter, R., & Bischoff, M. (2010). Numerical efficiency, locking and unlocking of NURBS finite elements. *Computer Methods in Applied Mechanics and Engineering*, *199*(5–8), 374–382.

18. Echter, R., Oesterle, B., & Bischoff, M. (2013). A hierarchic family of isogeometric shell finite elements. *Computer Methods in Applied Mechanics and Engineering*, *254*, 170–180.
19. Oesterle, B., Ramm, E., & Bischoff, M. (2016). A shear deformable, rotation-free isogeometric shell formulation. *Computer Methods in Applied Mechanics and Engineering*, *307*, 235–255.
20. Oesterle, B., Sachse, R., Ramm, E., & Bischoff, M. (2017). Hierarchic isogeometric large rotation shell elements including linearized transverse shear parametrization. *Computer Methods in Applied Mechanics and Engineering*, *321*, 383–405.
21. Bieber, S., Oesterle, B., Bischoff, M., & Ramm, E. (2022). Strategy for Preventing Membrane Locking Through Reparametrization. In: F. Aldakheel, B. Hudobivnik, M. Soleimani, H. Wessels, C. Weißenfels, & M. Marino (Eds.), *Current trends & open problems in computational mechanics* (pp. 61–73). Springer International Publishing.
22. Bieber, S., Oesterle, B., Ramm, E., & Bischoff, M. (2018). A variational method to avoid locking-independent of the discretization scheme. *International Journal for Numerical Methods in Engineering*, *114*(8), 801–827.
23. Fraeijs de Veubeke, B. (1965). *Stress analysis*. In: O. C. Zienkiewicz, & G. S. Holister (Eds.), (pp. 145–197). John Wiley & Sons.
24. Zienkiewicz, O. C. (2001). Displacement and equilibrium models in the finite element method by B. Fraeijs de Veubeke, Chapter 9, Pages 145–197 of Stress Analysis, Edited by O. C. Zienkiewicz and G. S. Holister, Published by John Wiley & Sons, 1965. *International Journal for Numerical Methods in Engineering*, *52*(3), 287–342.
25. Cook, R. D. (1974). Improved two-dimensional finite element. *Journal of the Structural Division*, *100*(9), 1851–1863.
26. Bieber, S., Auricchio, F., Reali, A., & Bischoff, M. (2023). Artificial instabilities of finite elements for nonlinear elasticity: Analysis & remedies. *International Journal for Numerical Methods in Engineering*, *124*(11), 2638–2675.
27. Bieber, S. (2024). *Locking and hourglassing in nonlinear finite element technology* [PhD thesis]. Institut für Baustatik und Baudynamik, Universität Stuttgart, Bericht Nr. 76.
28. Willmann, T., Bieber, S., & Bischoff, M. (2023). Investigation and elimination of nonlinear Poisson stiffening in 3d and solid shell finite elements. *International Journal for Numerical Methods in Engineering*, *124*(1), 235–263.
29. Müller, A., Vinod Kumar Mitruka, T. K. M., & Jakob, H. (2024). Ikarus v0.4. DaRUS (V1). University of Stuttgart.
30. Bischoff, M., & Ramm, E. (1997). Shear deformable shell elements for large strains and rotations. *International Journal for Numerical Methods in Engineering*, *40*(23), 4427–4449.
31. Klinkel, S., & Wagner, W. (1997). A geometrical non-linear brick element based on the EAS-method. *International Journal for Numerical Methods in Engineering*, *40*(24), 4529–4545.
32. Macneal, R. H., & Harder, R. L. (1985). A proposed standard set of problems to test finite element accuracy. *Finite Elements in Analysis and Design*, *1*(1), 3–20.

How to cite this article: Vinod Kumar Mitruka, T. K. M., & Bischoff, M. (2024). The mixed displacement method to avoid shear locking in problems in elasticity. *Proceedings in Applied Mathematics and Mechanics*, *24*, e202400129. https://doi.org/10.1002/pamm.202400129